NEOPLASIA
www.neoplasia.com

Volume 12 Number 2 February 2010 pp. 139–149 139

In Vivo Imaging of Xenograft Tumors Using an Epidermal Growth Factor Receptor–Specific Affibody Molecule Labeled with a Near-infrared Fluorophore[1]

Haibiao Gong, Joy Kovar, Garrick Little, Huaxian Chen and David Michael Olive

LI-COR Biosciences, Lincoln, NE, USA

Abstract

Overexpression of epidermal growth factor receptor (EGFR) is associated with many types of cancers. It is of great interest to noninvasively image the EGFR expression *in vivo*. In this study, we labeled an EGFR-specific Affibody molecule (Eaff) with a near-infrared (NIR) dye IRDye800CW maleimide and tested the binding of this labeled molecule (Eaff800) in cell culture and xenograft mouse tumor models. Unlike EGF, Eaff did not activate the EGFR signaling pathway. Results showed that Eaff800 was bound and taken up specifically by EGFR-overexpressing A431 cells. When Eaff800 was intravenously injected into nude mice bearing A431 xenograft tumors, the tumor could be identified 1 hour after injection and it became most prominent after 1 day. Images of dissected tissue sections demonstrated that the accumulation of Eaff800 was highest in the liver, followed by the tumor and kidney. Moreover, in combination with a human EGFR type 2 (HER2)–specific probe Haff682, Eaff800 could be used to distinguish between EGFR- and HER2-overexpressing tumors. Interestingly, the organ distribution pattern and the clearance rate of Eaff800 were different from those of Haff682. In conclusion, Eaff molecule labeled with a NIR fluorophore is a promising molecular imaging agent for EGFR-overexpressing tumors.

Neoplasia (2010) 12, 139–149

Introduction

The epidermal growth factor (EGF) receptor (EGFR, HER1, ErbB1) is a transmembrane protein of the tyrosine kinase receptor family. EGFR, together with human EGF receptor type 2 (HER2/ErbB2), HER3/ErbB3, and HER4/ErbB4, makes up the ErbB family of type 1 tyrosine kinases. EGFR protein contains an extracellular ligand-binding domain, a hydrophobic transmembrane domain, and an intracellular domain with tyrosine kinase activity [1,2]. EGFR plays an important role in physiological and pathological processes such as cell cycle progression, differentiation, apoptosis, migration, and invasion. Aberrant overexpression and/or activation of EGFR is associated with many types of cancers, including skin, breast, ovary, bladder, prostate, kidney, head and neck, and non–small cell lung cancers [2,3]. Various EGFR-targeted anticancer medicines have been developed by either targeting the extracellular ligand-binding domain through antibody blocking, or by inhibiting the tyrosine kinase activity using low–molecular weight molecules [4,5].

To assess the expression level of EGFR *in vivo*, noninvasive imaging methods have been developed. Most molecular imaging studies on EGFR exploited the specific binding between the receptor molecule and the anti-EGFR antibody. Successful imaging was achieved in both small animal tumor models [6–9] and human patients [10,11]. However, because of their large size (M_w, 150 kDa), these antibody-based imaging agents suffer from drawbacks such as long biodistribution time, poor penetrating capability, and slow clearance from the blood and normal tissues. EGF, the natural ligand for EGFR, has also been used to image EGFR expression *in vivo* [12–15]. Although the size of EGF (M_w, 6.2 kDa) is much smaller compared with those of antibodies,

Abbreviations: ABD, albumin-binding domain; EGF, epidermal growth factor; EGFR, EGF receptor; HER2, human epidermal growth factor receptor type 2; NIR, near-infrared; ROI, region of interest; TBR, tumor-to-background ratio

Address all correspondence to: Haibiao Gong, Ph.D., LI-COR Biosciences, Lincoln, NE 68504. E-mail: herbert.gong@licor.com

[1]This article refers to supplementary materials, which are designated by Figures W1 to W5 and are available online at www.neoplasia.com.

Received 25 August 2009; Revised 2 December 2009; Accepted 7 December 2009

DOI 10.1593/neo.91446

it stimulates the EGFR-mediated signaling pathways, which is an unwanted property for *in vivo* imaging [16].

Recently, emerging evidence has indicated that Affibody molecules could be good candidates as imaging agents. Affibody molecules are a class of affinity proteins composed of 58 amino acid residues that are derived from one of the immunoglobulin G (IgG)–binding domains of staphylococcal protein A. Several successful tumor imaging studies have been reported using HER2-specific Affibody molecules [17–20]. Affibody molecules binding specifically to EGFR have also been identified and characterized [21–24].

Owing to the reduced light absorption and scattering of near-infrared (NIR) light in animal tissues, and the low tissue autofluorescence in the NIR region, NIR optical imaging offers high sensitivity and signal-to-noise ratio compared with visible spectrum [25–27]. A variety of molecules labeled with NIR fluorophores have been successfully used for *in vivo* imaging. Some examples include 2-deoxyglucose [28,29], annexin V [30], RGD [31], EGF [13,14,16,32], and antibodies [7,33,34].

In this study, we evaluated the EGFR-specific Affibody (Eaff) labeled with a NIR fluorophore for *in vivo* optical imaging. The NIR fluorophore labeled EGFR-specific Affibody (Eaff800) was bound specifically by EGFR-overexpressing A431 cells. *In vivo* imaging study demonstrated that Eaff800 accumulated in A431 xenograft tumors, with the highest tumor-to-background ratio (TBR) achieved 1 day after probe administration. Moreover, we examined the specificity of Eaff800 *in vivo* by imaging with both Eaff800 and an HER2-specific Affibody labeled with another NIR fluorophore (Haff682). Results showed that Eaff800 and Haff682 accumulated in A431 tumor and HER2-overexpressing SKOV3 tumor, respectively. These results demonstrated that NIR fluorophore labeled Affibody molecules are promising agents for *in vivo* molecular imaging.

Materials and Methods

Chemicals and Reagents

The Affibody molecules were provided by Affibody AB (Bromma, Sweden). The Eaff molecule is in a head-to-tail dimeric form with a molecular weight of 13.7 kDa. The HER2-specific Affibody (Haff) molecule is a fusion protein of the HER2 monomer with the albumin-binding domain (ABD) and has a molecular weight of 12.1 kDa. IRDye800CW maleimide dye (Ex/Em: 774/789 nm) and IRDye800CW-labeled EGF (EGF800) were from LI-COR Biosciences (Lincoln, NE). TO-PRO-3 and SYTOX Green nucleic acid stain reagents were purchased from Invitrogen (Carlsbad, CA). DY-682 maleimide dye, Recombinant human EGF and TCEP·HCl was purchased from Dyomics (Jena, Germany), R&D Systems (Minneapolis, MN), and Fisher Scientific (Pittsburgh, PA), respectively.

Conjugation of Affibody Molecules with NIR Dyes

The Affibody used in this study contains a unique C-terminal cysteine residue for thiol-reactive maleimide dye labeling. To reduce the spontaneously formed disulfide bond between the cysteine residues, the Affibody molecules were incubated with 5 mM TCEP·HCl. The excess TCEP·HCl was removed by passing the reaction mixture through a Zeba Spin Desalting Column (Fisher Scientific). The maleimide dye was reconstituted in DMSO to a concentration of 10 mM and added to the Affibody solution. The reaction mixture was incubated at room temperature for 3 hours before passing through another Zeba Spin Desalting Column to remove free dye. The concentrations of labeled Affibody molecules and the labeling efficiency were calculated based on the absorbance at 280 nm and 778 nm (IRDye800CW) or 688 nm (DY-682), respectively.

Cell Culture

The human skin epidermoid carcinoma cell line A431, ovarian adenocarcinoma cell line SK-OV-3 (SKOV3), and breast adenocarcinoma cell lines MDA-MB-231 (MDA231) and SK-BR-3 (SKBR3) were obtained from the American Type Culture Collection (ATCC, Manassas, VA). A431 and MDA231 cells were maintained in Dulbecco's modified Eagle medium (DMEM) supplemented with 10% fetal calf serum and 1% penicillin-streptomycin (complete DMEM). SKOV3 and SKBR3 cells were maintained in McCoy 5A medium (McCoy) supplemented with 10% fetal calf serum and 1% penicillin-streptomycin (complete McCoy).

To collect cell lysates for Western blot analysis, cells were rinsed with PBS and lysed with radioimmunoprecipitation assay buffer. When treatment with Eaff or EGF was necessary, the agents were diluted in serum-free medium to the desired concentrations and added to the cells. After incubation at 37°C for 2 hours, cells were rinsed with PBS and lysed with radioimmunoprecipitation assay buffer.

Western Blot

The Western blot analysis was performed as previously described with modifications [35]. In brief, protein samples were denatured by boiling for 5 minutes and loaded onto 10% Bis-Tris gels. After electrophoresis, proteins were transferred to nitrocellulose membranes. Membranes were blocked for 2 hours with Odyssey Blocking Buffer, then incubated for 1 hour with primary antibodies diluted in Odyssey Blocking Buffer. The mouse EGFR antibody, mouse P44/42 mitogen-activated protein kinase (MAPK) (ERK1/2) antibody, rabbit phospho-EGFR (Tyr1045) antibody, rabbit phospho-P44/42 MAPK (ERK1/2) antibody, and rabbit HER2/ErbB2 antibody were purchased from Cell Signaling Technology (Danvers, MA). The mouse pan-Actin antibody was purchased from NeoMarkers (Fremont, CA). Two primary antibodies from different species (such as mouse anti–P44/42 and rabbit anti–phospho-P44/42) were added together.

After incubating with primary antibodies, the membranes were washed with PBS containing 0.1% Tween 20 (PBST) three times. Then the membranes were incubated for 1 hour with IRDye800CW-conjugated goat antirabbit IgG and IRDye680-conjugated goat antimouse IgG secondary antibodies (LI-COR Biosciences) diluted in Odyssey Blocking Buffer. The blots were then washed three times with PBST and rinsed with PBS. Proteins were visualized by scanning the membrane on an Odyssey Infrared Imaging System (LI-COR Biosciences) with both 700- and 800-nm channels.

Cell Binding and Uptake Assay

Cells were seeded at approximately 3×10^4 (A431), 2×10^4 (MDA231 and SKBR3), or 1×10^4 (SKOV3) cells per well in 96-well plates and cultured overnight before the assay. The cell density was approximately 70% to 80% confluent at the time of assay. The NIR fluorophore–labeled targeting agents were diluted in complete cell culture medium to designated concentrations and incubated in the 37°C incubator for 2 hours except where otherwise stated. For competition study, unlabeled agents were diluted in complete medium and incubated with the cells for 1 hour. The competitors were then removed before adding targeting agents. After incubating with targeting agents, cells were fixed with 3.7% formaldehyde/PBS and washed with PBST. The cells were then incubated in TO-PRO-3 stain agent (1:5000 in PBS) to normalize for

cell numbers. After three additional washes with PBST, the plate was scanned and signal intensity quantified [36].

Microscopic Analysis

Cells were seeded in eight-well chamber slides (Nalge Nunc International Corp, Naperville, IL) and cultured overnight. The cells were incubated with 20 nM targeting agent at 37°C for 2 hours, fixed, and washed as previously described. Instead of TO-PRO-3, SYTOX Green nucleic acid stain agent was used to visualize the nuclei by microscopy. After the final wash, the slides were mounted with Fluoromount reagent (Sigma, St Louis, MO). The images were acquired using a Leica DM6000b Bio/Med microscope system (Leica Microsystems, Inc, Bannockburn, IL) equipped with a xenon lamp. The excitation and emission filters used for NIR imaging are HQ760/40 and HQ830/50 (Chroma Technology Corp, Rockingham, VT), respectively. The images were deconvolved using the accompanying software.

Xenograft Mouse Model

All animals were cared for and maintained under the supervision and guidelines of the University of Nebraska-Lincoln Institutional Animal Care and Use Committee. Mice were maintained on a purified maintenance diet (AIN-93M) from Harlan Teklad (Madison, WI). The xenograft tumors were established as previously described with modifications [37]. In brief, athymic nude (*nu/nu*) mice, obtained from Charles River Laboratories, Inc (Cambridge, MA) at 4 weeks of age, were subcutaneously injected with suspension cells in 0.1 ml of serum-free medium. The numbers of cells injected was 10^6 or 5×10^6 for A431 or SKOV3, respectively. To establish both A431 and SKOV3 tumors on the same mouse, SKOV3 cells were inoculated 1 week before inoculating A431 cells to achieve similar tumor growth.

In Vivo *Animal Imaging*

Mice were anesthetized with 2% isoflurane throughout the procedures. For imaging experiments, the contrast agent was diluted in 100 μl of PBS and injected through the tail vein. The images were acquired at the indicated time points with a Pearl Imager (LI-COR Biosciences). The Ex/Em settings for the 700- and 800-nm channels were 685/720 and 785/820 nm, respectively. A cooled charge-coupled device camera was used to collect the images. The images were analyzed using the accompanying software. Regions of interest (ROIs) for both tumor and contralateral areas (background) were selected from equivalent-sized areas containing the same number of pixels. ROIs were quantified for mean pixel values. TBR was derived by dividing mean tumor signal by mean background signal [28].

Organ and Tissue Analysis

Mice were killed 1 day after imaging agent injection and dissected to collect the organs. The excised organs were rinsed in PBS, and imaged using a Pearl Imager. The organs were then snap-frozen in OCT compound for cryosectioning. Sections (8-μm thickness) were scanned on an Odyssey Infrared Imaging System for the targeted fluorescence signal. To compare the fluorescence signal on tissue sections, ROIs were drawn on the tissue sections and blank regions of the slides. The signal intensity was calculated as the average signal intensity on the tissue region minus the average signal intensity on the blank region.

Results

The Effect of Eaff on EGFR and ERK1/2 Phosphorylation

It is known that activation of the EGFR tyrosine kinase activity leads to the phosphorylation of a variety of target proteins, including ERK1/2 and EGFR itself [38]. To evaluate whether Eaff stimulates EGFR-mediated signaling pathways, A431 cells were treated with 5 or 20 nM Eaff. In contrast to EGF, which stimulated the phosphorylation of both proteins in a dose-dependent manner, Eaff treatment did not change the phosphorylation level of EGFR and ERK1/2 (p44/p42 MAPK). However, a high concentration of Eaff (100 nM), when applied together with 5 nM EGF, compromised the stimulatory effect of EGF on EGFR and ERK1/2 phosphorylation (Figure 1).

Specific Cellular Binding and Uptake of Labeled Affibody Molecules

Because the Affibody monomer molecule contains five to six lysine residues [19,39], conjugation of dye molecules to lysine may result in heterogeneous multiple labeling. It is also possible to disturb the binding motif by attaching a dye molecule to its internal lysine residues. To avoid this problem, the Affibody molecules were conjugated with the maleimide dye to its C-terminal cysteine. The incorporation of dye into the Affibody molecules was monitored by gel electrophoresis (Figure W1). The NIR fluorophore–labeled Affibody molecules were designated as Eaff800 (Eaff labeled with IRDye800CW), Eaff682 (Eaff labeled with DY-682), Haff800 (Haff labeled with IRDye800CW), and Haff682 (Haff labeled with DY-682), respectively.

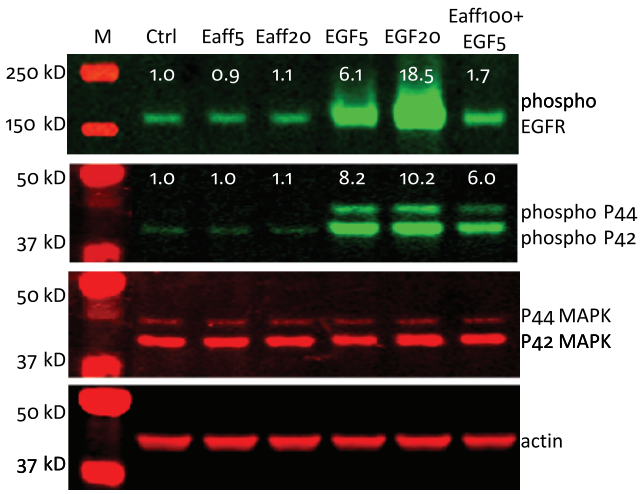

Figure 1. The effect of EGF and EGFR-specific Affibody (Eaff) on EGFR-mediated phosphorylation of EGFR and ERK1/2 (P44/42 MAPK) proteins. A431 cells were treated with either Eaff or EGF. Two concentrations (5 and 20 nM) for both Eaff (Eaff5 and Eaff20) and EGF (EGF5 and EGF20) were used. A combination of high-concentration Eaff (100 nM, Eaff100) and 5 nM EGF was also used to treat cells. P44/42 MAPK and actin were used as internal controls. The relative expression levels were calculated by dividing the signal intensities of phospho-EGFR or phospho-P44/P42 by actin signal intensities. Note that the molecular weight markers in the second panel (phospho-P44/P42) and the third panel (P44/P42 MAPK) were the same. *Ctrl* indicates control without drug treatment.

To compare the protein expression levels of EGFR and HER2 in various cell lines, cell lysates of MDA231, A431, SKOV3, and SKBR3 cells were analyzed by Western blot. Both EGFR and HER2 proteins were detected in these cell lines. However, the EGFR level was much higher in A431 cells than in any other cell lines, whereas HER2 was highly expressed in SKOV3 and SKBR3 cells (Figure 2*A*). This finding was consistent with previous reports on EGFR and HER2 expression [40]. These cell lines were also used to investigate the binding specificity of EGFR and HER2-specific Affibody molecules. The binding and uptake assay was performed by incubating 5 nM Eaff800 or Haff800 with MDA231, A431, SKOV3, and SKBR3 cells. Results demonstrated that whereas A431 cells contained high Eaff800 signal, there was only minimal Eaff800 binding and uptake for MDA231, SKOV3, or SKBR3 cells. On the contrary, the HER2-specific Haff800 showed the strongest signal in SKOV3 and SKBR3 cells, and the signal in MDA231 and A431 cells was low (Figure 2*B*). On the basis of these results, the A431 cells and SKOV3 cells were selected as EGFR- and HER2-overexpressing cells, respectively, for subsequent studies.

The binding and uptake of Eaff800 by A431 cells were dependent on Eaff800 concentration. With the increase of Eaff800 concentration, the signal intensity also increased (Figure 2*C*), with the maximum signal obtained at approximately 20 to 50 nM. As a comparison, the same concentrations of Haff800 and free IRDye800CW dye were incubated with A431 cells at the same condition. The signals from these agents were minimal, even at a concentration as high as 100 nM (Figure 2*C*).

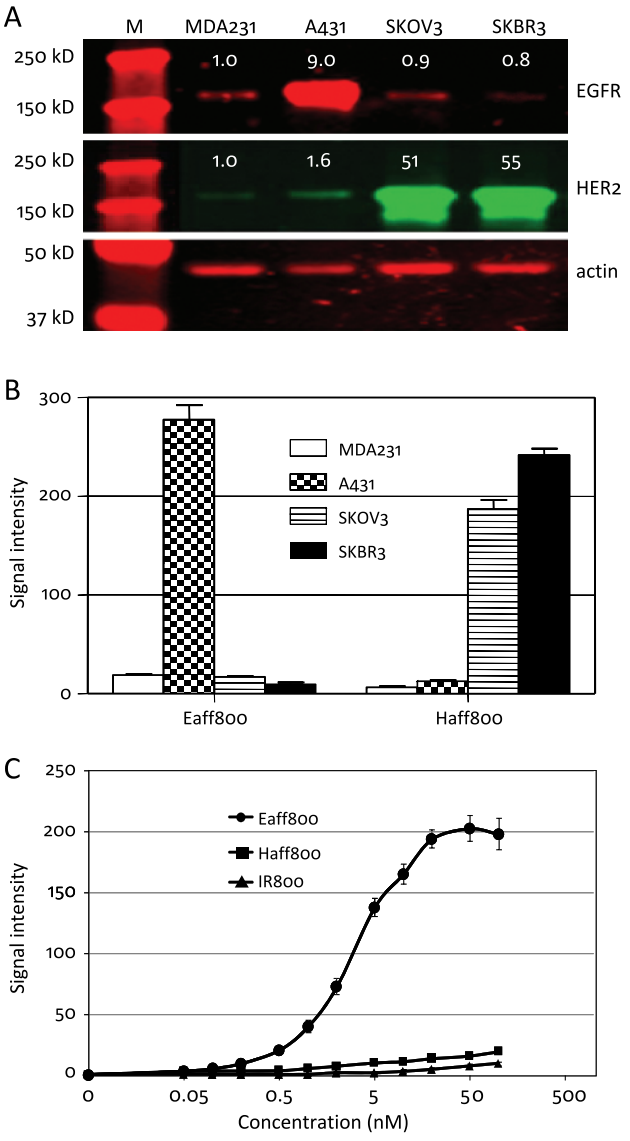

Figure 2. Specific binding and uptake of IRDye800CW-labeled Affibody molecules. (A) The protein expression levels of EGFR and HER2 in MDA-MB-231 (MDA231), A431, SKOV3, and SKBR3 cells. Actin served as an internal control. The relative expression levels were calculated by dividing the signal intensities of EGFR or HER2 by actin signal intensities. (B) The binding and uptake of EGFR-specific Eaff800 and HER2-specific Haff800 by MDA231, A431, SKOV3, and SKBR3 cells. (C) Concentration-dependent binding and uptake of Eaff800-, Haff800-, or IRDye800CW-free dye by A431 cells.

Comparison of Eaff800 with EGF800

NIR fluorophore–labeled EGF has been used as an imaging agent [13,14]. So it was of interest to compare Eaff and EGF labeled with the same NIR fluorophore. Both Eaff800 (5 nM) and EGF800 (5 nM) were diluted in complete DMEM and incubated with A431 cells for different periods. As shown in Figure 3*A*, the binding and uptake of EGF800 was faster than that of Eaff800, and the signal intensity of EGF800 was higher in the early stage. Before 1 hour, the binding and uptake of both agents increased over time. At the 1-hour time point, binding and uptake of EGF800 decreased, whereas the Eaff800 signal continued to increase. The Eaff800 signal reached its highest level at 4 to 6 hours and declined thereafter (Figure 3*A*).

Competition analysis was performed by incubating different concentrations of unlabeled Eaff or EGF with A431 cells before adding targeting agents. Both Eaff and EGF blocked the binding and uptake of Eaff800. The blocking effect of Eaff and EGF was observed at a concentration as low as 5 nM, which was the same concentration as Eaff800 used in this assay. With the increase of competitor concentrations, the Eaff800 signal declined. However, the competition effect of Eaff was more prominent than that of EGF, especially at concentrations higher than 20 nM (Figure 3*B*). It was also noted that both Eaff and EGF blocked the binding and uptake of EGF800 by A431 cells (data not shown).

The localization of Eaff800 and EGF800 in A431 cells were examined by microscopy. For both Eaff800 and EGF800, intense signals were associated with the cell membrane. However, foci probably representative of internalized agents were also observed inside the cells (Figure 3*C*).

Targeting EGFR-Overexpressing Xenograft Tumors by Eaff800

Eaff800 probe was tested in mouse xenograft tumor models by *in vivo* imaging. Nude mice bearing A431 xenograft tumors were injected with 0.5 nmol of Eaff800 through the tail vain. Whole mouse images were acquired at different time points after agent administration. Figure 4*A* showed a series of these images (dorsal view). Intense signal was found in the region where the kidney is located. The belly view of the mouse also revealed high signal intensity at the liver region (data not shown). The accumulation of Eaff800 signal in the liver and kidney was confirmed by imaging dissected organs, as discussed later. The tumor could be identified at 1 hour after probe injection and it became most prominent after 1 day (approximately 24 hours). Quantification of the ROIs of equivalent-sized areas from the tumor and contralateral region showed

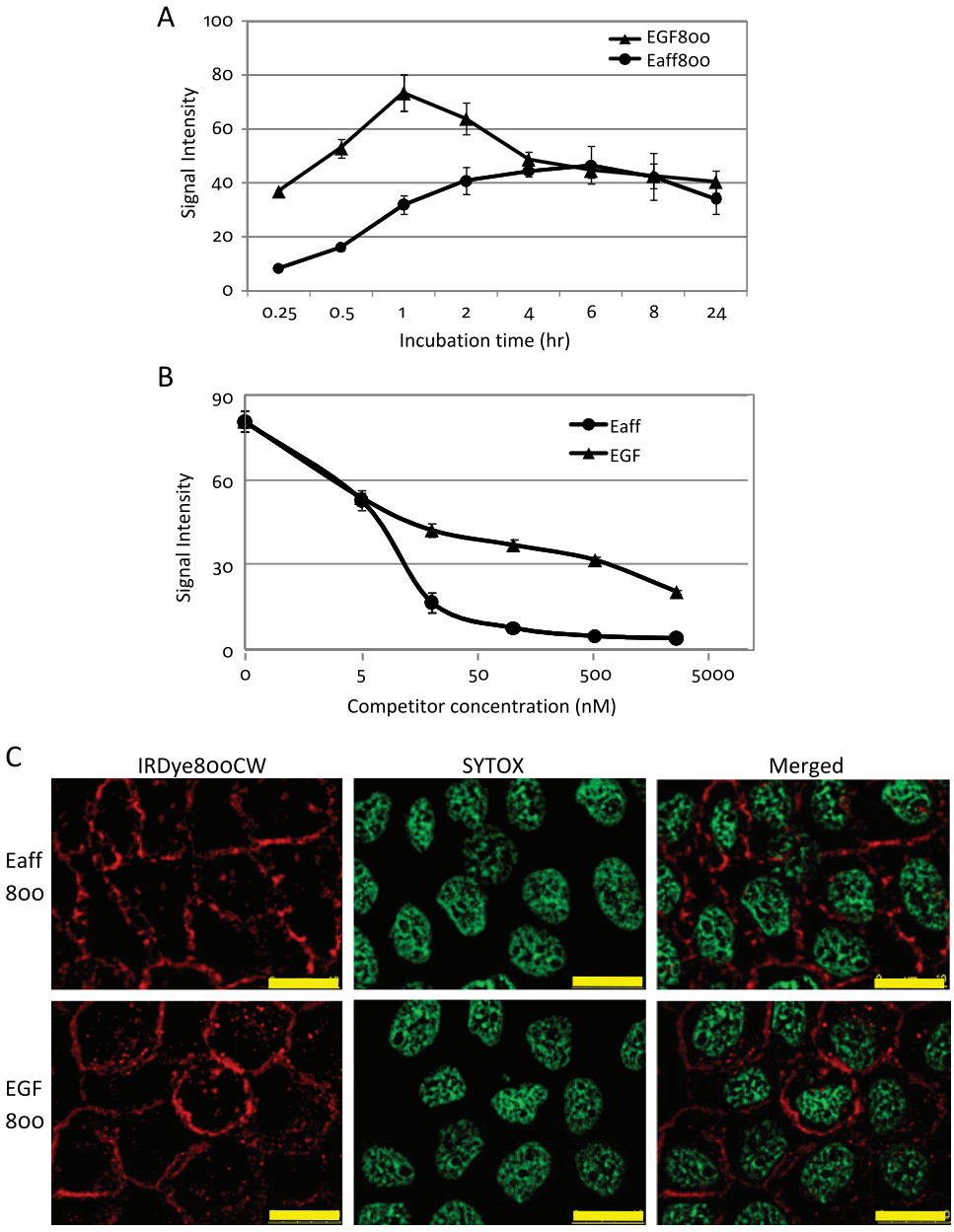

Figure 3. The comparison of cellular binding and uptake between Eaff800 and EGF800. (A) Binding and uptake time course of Eaff800 (5 nM) and EGF800 (5 nM) by A431 cells. (B) The blocking of Eaff800 (5 nM) binding by increasing concentrations of unlabeled Eaff or EGF. (C) Microscopic examination of Eaff800 (20 nM) and EGF800 (20 nM) binding and uptake by A431 cells. Sytox green was used to stain the nuclei. Scale bar, 10 μm.

that the signal intensities of both tumor and normal tissue peaked at 20 minutes after agent injection. Thereafter, the signal decreased over time (Figure 4*B*). The signal decline was more dramatic in normal tissues, especially during the period from 6 to 48 hours, resulting in an increased TBR, which reached the highest level at 24 hours (Figure 4*C*). At 96 hours, most of the agent was cleared out of the body. The residual signals in the tumor and normal tissue were 8.7 ± 0.5% and 5.7 ± 1.0% of those at the highest levels (20 minutes after agent injection), respectively.

To investigate the accumulation of imaging agent in different organs, mice were killed 1 day after agent injection. The organs were collected and imaged. Consistent with *in vivo* imaging observations, signal intensities were high in the liver, kidney, and tumor (Figure 5*A*). These organs were then snap-frozen in OCT compound, sectioned at 8-µm thickness, and scanned. Quantification of tissue section revealed the strongest signal in the liver, followed by the kidney and tumor. All other tissues contained only a low level of signal (Figure 5, *B* and *C*). Interestingly, unlike the even distribution of Eaff800 in the liver, a higher Eaff800 signal was located in the renal cortex of the kidney compared with other regions (Figure 5*B*).

Two-color In Vivo *Imaging Using Eaff800 and Haff682*

Haff conjugated with Alexa Fluor 750 was successfully used for optical imaging [18]. Before animal injection, Eaff800 and Haff682 were added together to A431 cells or SKOV3 cells to examine whether the Affibody molecules interfere with each other's binding. Compared with the binding and uptake of individual probes, no significant difference

was observed when two probes were added together (data not shown), indicating the lack of cross reactivity.

To test the *in vivo* specificity of labeled Affibody molecules, 100 μl of imaging agent solution containing 0.5 nmol of Eaff800 and 0.5 nmol of Haff682 was injected into nude mice bearing both A431 tumors and SKOV3 tumors through the tail vain. Multiple-color images were acquired 1 day after agent injection. As expected, A431 tumors contained a higher Eaff800 signal (Figure 6*A-a*), whereas SKOV3 tumors contained a higher Haff682 signal (Figure 6*A-b*). The merged picture displayed a two-color image representing selective accumulation of two different probes (Figure 6*A-d*). The A431 tumor on the left side is *green*, which represented predominant Eaff800 signal, and the SKOV3 tumor on the right side is *red*, which represented predominant Haff682 signal. The TBRs for A431 tumor and SKOV3 tumor were 1.7 ± 0.2 and 2.1 ± 0.3, respectively. Because pseudocolored images can distinguish different intensities easier, the mouse images with Eaff800 signal or Haff682 signal were also presented in pseudo color (Figure W2). Images of tumor sections also demonstrated that Eaff800 and Haff682 accumulated preferably in A431 tumors and SKOV3 tumors, respectively (Figure 6*B*).

Next, we exchanged the labeling, that is, Eaff was labeled with DY-682 (Eaff682), and Haff was labeled with IRDye800CW (Haff800). As expected, Eaff682 accumulated in A431 tumor and Haff800 accumulated in SKOV3 tumor predominantly (Figure W3).

Whereas both probes specifically targeted their respective tumors, the organ distribution pattern and the clearance rate of Eaff800 and Haff682 were different. Whole body images showed predominant Eaff800 signal (*green*) in the liver region (Figure 6*A-d*). The accumulation of Eaff800 in the liver was confirmed by images of dissected organs (Figure W4*A*). Analysis of tissue sections revealed that the liver-to-kidney ratio of Eaff800 signal was approximately 3.8 (Figure W4, *B* and *C*), which is similar to the result when Eaff800 alone was injected (liver-to-kidney ratio = 3.5). However, the signal intensities of Haff682 in the liver and kidney were comparable (liver-to-kidney ratio = 1.1; Figure W4, *B* and *C*). The clearance rate of Eaff800 was faster than

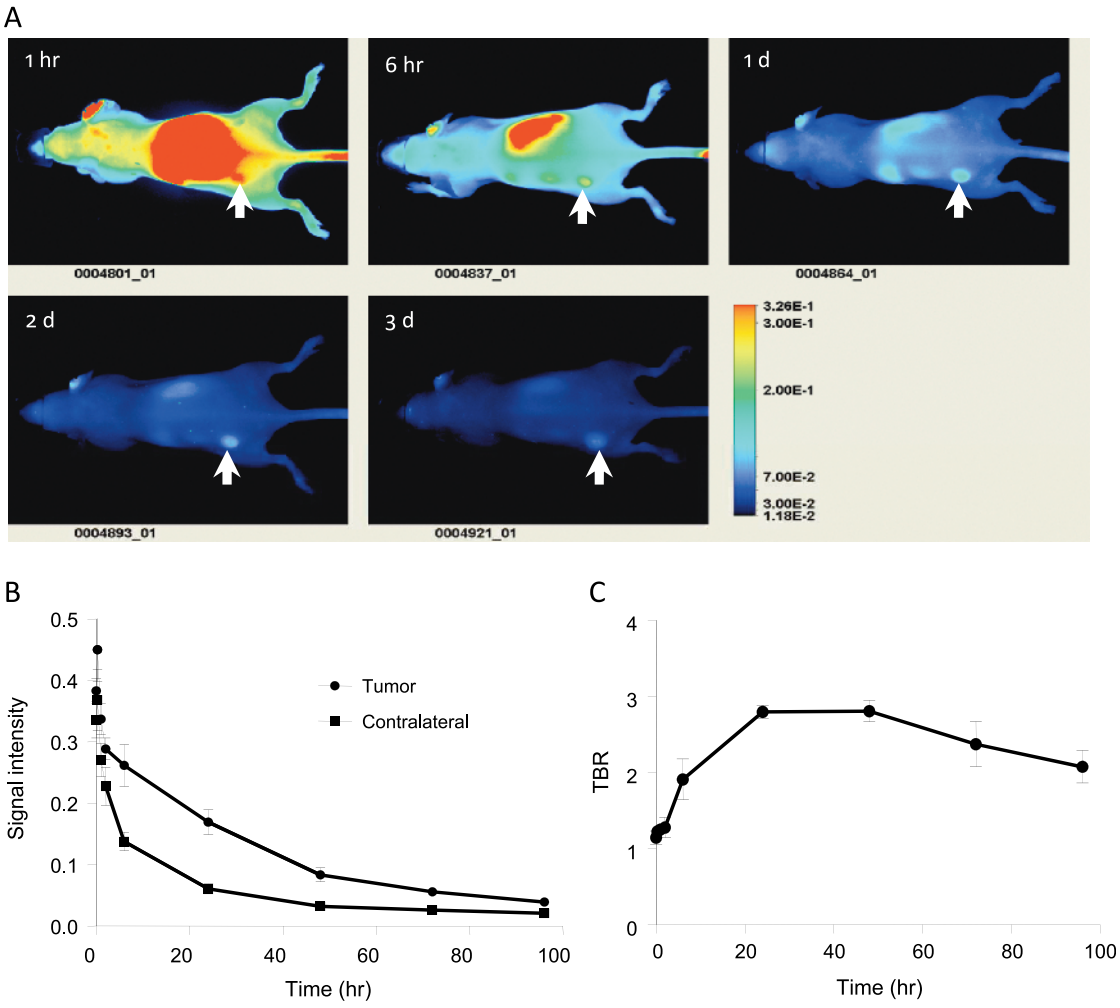

Figure 4. *In vivo* optical imaging of nude mice bearing A431 tumors using Eaff800. (A) A representative series of whole body images (dorsal view) acquired at different time points after injection of 0.5 nmol of Eaff800. The tumors were indicated with arrows. (B) Clearance of Eaff800 from the tumor and normal tissue. Average signal intensities were quantified using ROIs of equivalent-sized areas from the tumor sites and contralateral sites at indicated time points. Data were presented as mean ± SD of three individual mice. (C) TBR at different time points after probe injection. TBR was calculated by dividing the mean tumor signal by the mean background signal of the contralateral site.

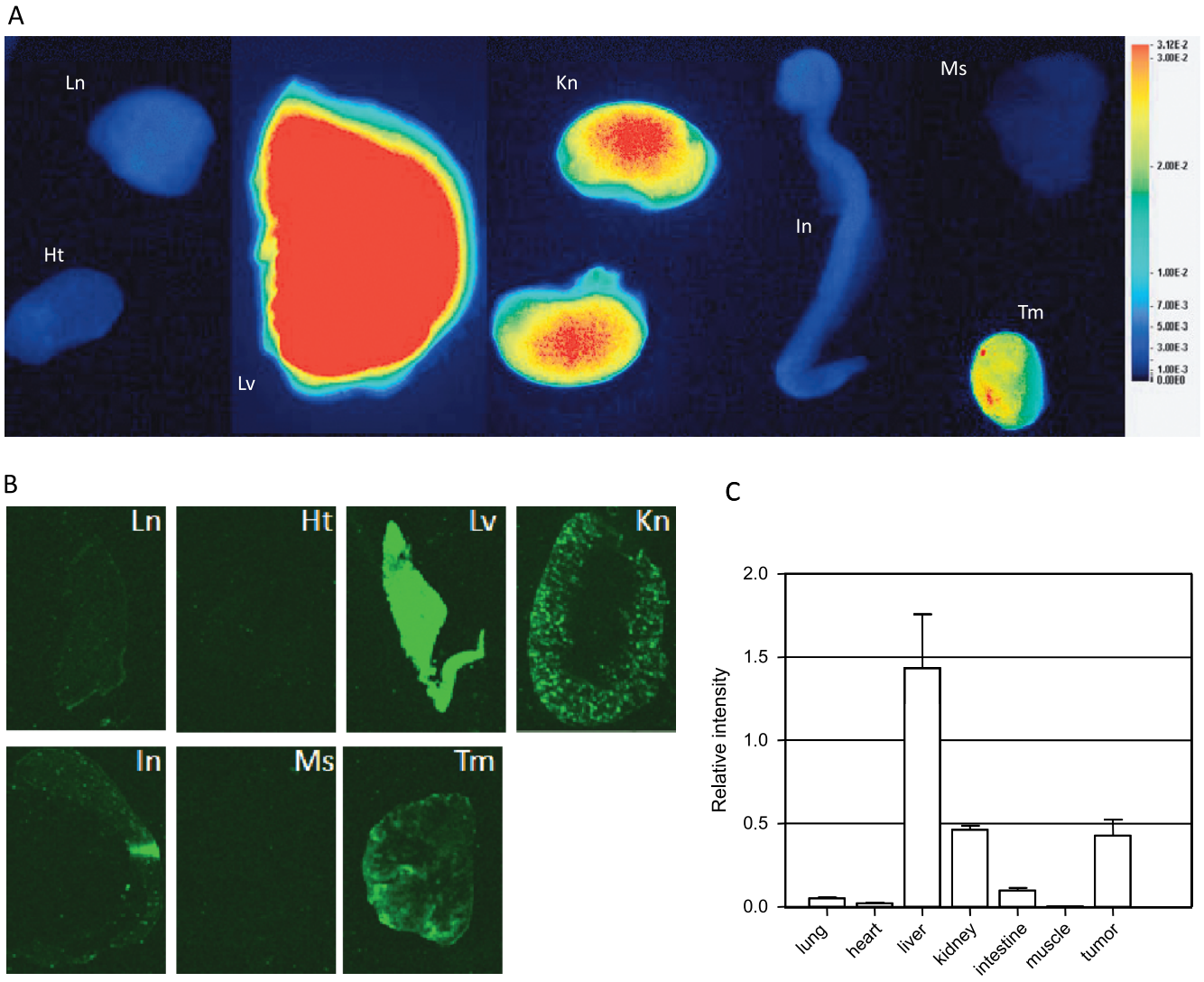

Figure 5. Tissue distribution of Eaff800. (A) Nude mice bearing A431 tumors were killed 1 day after Eaff800 injection. The organs were collected and rinsed in PBS before imaging. *Ht* indicates heart; *In*, intestine; *Kn*, kidney; *Ln*, lung; *Lv*, liver; *Ms*, muscle; *Tm*, tumor. Note that the liver was imaged separately and merged to the picture because the liver signal was so strong that it illuminated the surrounding tissues if imaged together. (B) Fluorescence images of cryosections of dissected organs. The organs were snap-frozen in OCT compound and sectioned at 8-μm thickness. (C) Quantification of signal intensities of tissue sections. Average signal intensities were calculated using ROIs from different tissue sections.

that of Haff682. At 1 day after probe administration, the signal intensity of Eaff800 as measured by whole body imaging decreased to 11.1 ± 0.6% of the highest level (20 minutes after agent injection), whereas residual signal of Haff682 still remained 57.9 ± 1.2% of the highest level.

When Eaff682 and Haff800 were used, more Eaff682 accumulated in the liver (Figure W5), revealing that the accumulation of Eaff in the liver was independent of the fluorophore conjugated.

Discussion

In vivo molecular imaging has become a valuable tool in biomedical research and drug development [41,42]. The radionuclide-based imaging technologies, such as positron emission tomography and single photon emission computed tomography, have been used in clinical applications. In the research field, fluorescence optical imaging is becoming more and more popular owing to its low cost, ease of use, longer time window for image capture, and ability to track multiple probes simultaneously. Compared with the visible spectrum, the NIR fluorochrome reduces the autofluorescence, maximizes tissue penetration, and is ideally suitable for noninvasive animal imaging [25,27]. In this study, we labeled the Affibody molecules with organic NIR fluorescent dyes and characterized these labeled molecules for *in vivo* optical imaging. In contrast to some studies in which probes with different labeling (fluorescent dyes or radionuclide) were used for *in vitro* cell based assays and *in vivo* imaging [19,33,39,43], we demonstrated here that one probe labeled with NIR fluorophore can be used throughout the study, from plate-based binding and uptake assay, microscopic analysis, to *in vivo* animal imaging. Apparently, this will significantly reduce the working load and cost.

One challenge for molecular imaging is to develop target-specific imaging agents. A variety of NIR probes labeled with organic dyes or quantum dots has been developed to track molecular and cellular

events *in vivo* [25,41]. Although these probes have been proven successful for *in vivo* imaging, they are of different origins and function based on different mechanisms. As a consequence, different strategies for development and characterization were needed for different targets, complicating the imaging application. Affibody molecules specific to different targets can be selected from the same library. Because these molecules differ from each other by only 13 amino acids [21], the labeling and characterization procedure could be standardized, thus greatly facilitating the development of imaging agents. In this study, we took advantage of the unique cysteine that is purposely engineered to the C-terminus of Affibody molecules for maleimide dye conjugation. This strategy avoided the problem of multiple heterogeneous labeling in the case of *N*-hydroxysuccinimide dye conjugation. As a result, the labeling was homogeneous and reproducible.

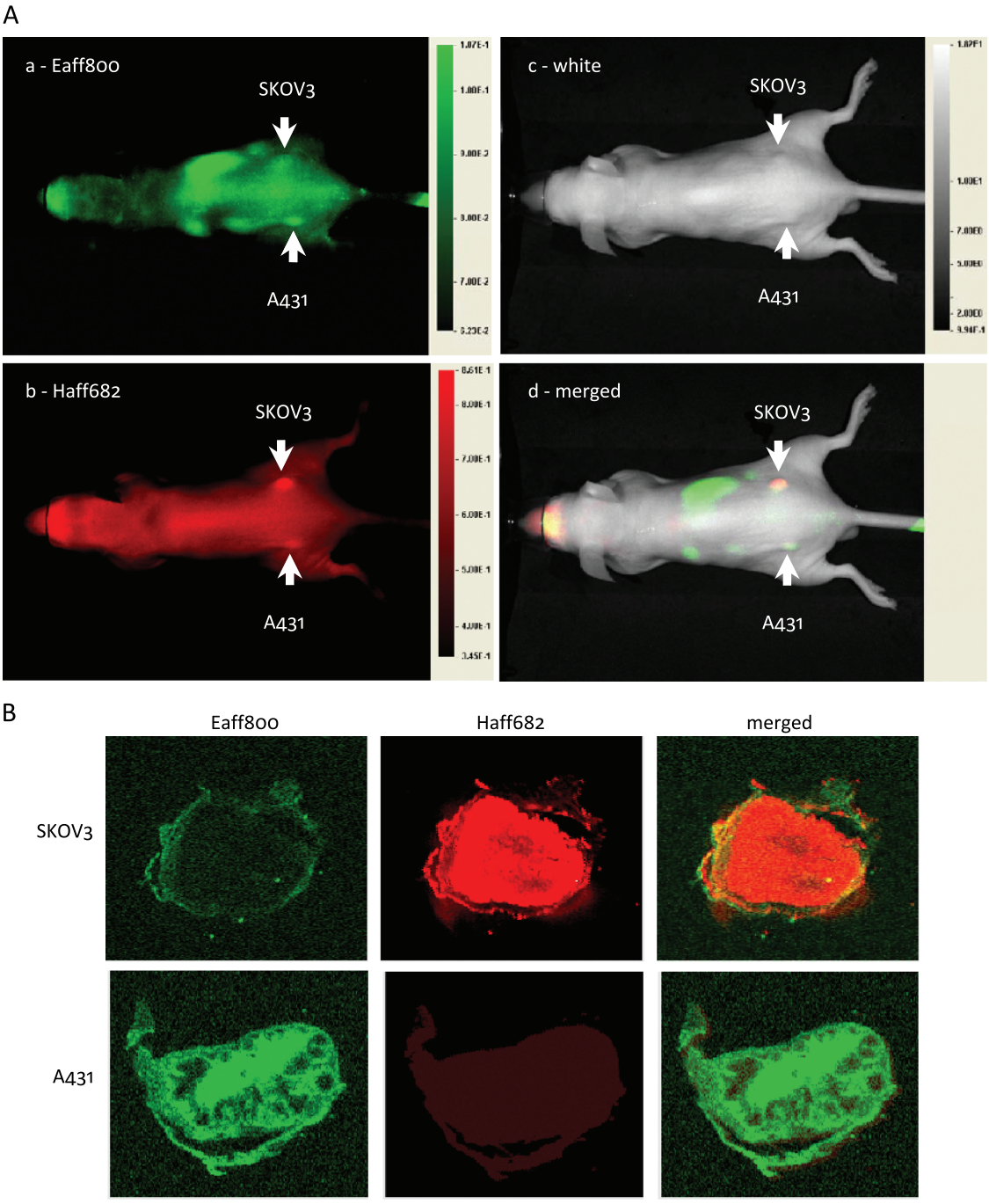

Figure 6. Two-color *in vivo* optical imaging with Eaff800 and Haff682. (A) Nude mice bearing A431 and SKOV3 tumors on the left and right sides, respectively, were injected with 100 μl of PBS containing 0.5 nmol of Eaff800 and 0.5 nmol of Haff682. Whole body images (dorsal view) were acquired 1 day after agent injection. Green and red represent IRDye800CW and DY-682 fluorescence signals, respectively. The tumors were indicated with arrows. (B) Fluorescence images of cryosections of A431 and SKOV3 tumors. Mice bearing A431 and SKOV3 tumors were killed 1 day after agent injection. The tumors were snap-frozen in OCT compound and sectioned at 8-μm thickness.

The biologic properties of the labeled Affibody molecules were evaluated by *in vitro* cell-based assays. The labeled molecules were taken up by cells expressing the respective targets (Figure 2*B*), demonstrating good specificity. Furthermore, no cross-interference was observed when two Affibody molecules (Eaff800 and Haff682) were added together. The specificity of Eaff800 was confirmed by the competition assay. The cellular binding and uptake of Eaff800 by A431 cells was inhibited by preincubation of unlabeled Eaff or EGF in a dose-dependent manner (Figure 3*B*). The competition between Eaff and EGF indicated that the binding sites of these two molecules on EGFR may be close to each other. The occupation of one molecule to its binding site interferes with the binding of the other molecule. The competition between Eaff and EGF may also explain the blocking effect of Eaff on EGF-stimulated EGFR and ERK1/2 phosphorylation.

An ideal imaging agent should not interfere with the signaling pathways mediated by the imaging target. Out data showed that Eaff did not stimulate EGFR-mediated phosphorylation of EGFR and ERK1/2 proteins (Figure 1). This offers an advantage over EGF, which is known to stimulate EGFR signaling pathways, resulting in the modulation of cell proliferation and tumorigenesis [44].

In vivo study showed that Eaff800 was rapidly localized in the A431 tumor after intravenous injection. Although the tumor was most clearly visualized after 1 day of probe injection, the tumor location could be identified from the background as early as 1 hour and remained clear after 3 day (Figure 4). This wide time window of image acquisition provides an advantage over radionuclide probes, whose image acquisition normally needs to be completed within hours [10,15,17,19,23]. The stable signal of the fluorescent dye also makes it suitable for longitudinal monitoring of probe distribution and clearance over time. It was reported recently that indium 111 (^{111}In)–labeled monomeric EGFR-specific Affibody performed better compared with the dimeric form for tumor imaging [24]. It would be of interest to test whether this is true in the case of NIR fluorophore labeling.

It has been reported that Affibody molecules labeled with radionuclide accumulated in the kidney [19,20,24]. Our results also revealed that the kidney retained high levels of Haff682 and Eaff800 signals after 1 day of probe administration (Figure 5). However, the organ distribution pattern of Eaff800 was different from that of Haff682. The ratio of liver signal to kidney signal was much higher for Eaff800 compared with that for Haff682, indicating a preferable accumulation of Eaff800 in the liver. This high uptake of Eaff800 by the liver is independent of the f luorescent dye conjugated to the Affibody molecule, as Eaff labeled with DY-682 (Eaff682) also accumulated preferably in the liver. The high liver uptake is likely due to the specific binding of Eaff to mouse EGFR, which is expressed in liver cells [45]. This high liver uptake of Eaff800 is in contrast to the observation in the study using the EGFR-specific Affibody labeled with ^{111}In, in which kidney was shown to be the prominent organ of radioactivity accumulation [24]. The possible explanation for this discrepancy might be the labeling difference (fluorescent dye *vs* radionuclide). However, further investigation is needed to clarify this point.

Fluorescence optical imaging has the advantage of multiple channels, which can be used to image two or more targets simultaneously [7,46]. It has been reported that five different fluorophores were simultaneously used to visualize primary draining lymph nodes [47]. Whereas this may be useful for imaging small animals, it will not be practical for human clinical use. The instruments currently available for human clinical imaging such as the Zeiss Pentero as well as instruments currently under development are focused on using wavelengths solely in the NIR region between 700 and 850 nm. In the current study, we labeled EGFR- or HER2-specific Affibody molecules with two NIR fluorophores, respectively. The specific uptake of the two probes by EGFR- or HER2-overexpressing tumors was revealed by two-color imaging (Figure 6). It was noted that low levels of Eaff800 and Haff682 signals were also detected in SKOV3 tumor and A431 tumor, respectively. This undesirable signal might be caused by the binding of Eaff800 and Haff682 to low levels of EGFR in SKOV3 and HER2 in A431, respectively. Nonspecific binding of probes might also contribute to this nontargeted tumor accumulation. In principle, this two-color imaging method can be applied to detect and differentiate any types of tumors that overexpress unique cell markers. It is worth noting that the tumors in the two-color imaging experiment were smaller than those used in other similar studies. The mean tumor weights were 13.3 ± 5.9 and 11.8 ± 2.1 mg for A431 and SKOV3 tumors, respectively. As a comparison, the tumor weights in other studies were between 100 and 300 mg [18,48]. These results demonstrated the capability of Eaff800 and Haff682 to identify small tumors at early stages.

It has been known that fusion of ABD to imaging probes could prolong the circulation half-life of the probes [43]. The ABD effect might account for the slow clearance of Haff800, which contains an N-terminal ABD [49]. Studies also demonstrated that fusion of an ABD to an HER2-specific Affibody improved the performance of the Affibody as an optical imaging agent [18]. It would be interesting to see whether the same strategy can be applied to the Eaff molecule to further improve its performance.

In conclusion, we reported here the development and characterization of an optical imaging agent Eaff800. This agent was based on an Affibody molecule specifically binding to EGFR and labeled with a NIR fluorophore. The specificity of Eaff800 was examined by *in vitro* cell binding and uptake analysis and confirmed by targeting EGFR-overexpressing tumors in xenograft mouse models. Moreover, in combination with an HER2-specific probe Haff682, Eaff800 could be used to distinguish between EGFR- and HER2-overexpressing tumors.

Acknowledgments

The authors thank Affibody AB (Bromma, Sweden) for providing Affibody molecules.

Conflicts of Interest

The authors are employees at LI-COR Biosciences.

References

[1] Ferguson KM, Darling PJ, Mohan MJ, Macatee TL, and Lemmon MA (2000). Extracellular domains drive homo- but not hetero-dimerization of erbB receptors. *EMBO J* **19**, 4632–4643.

[2] Kari C, Chan TO, Rocha de Quadros M, and Rodeck U (2003). Targeting the epidermal growth factor receptor in cancer: apoptosis takes center stage. *Cancer Res* **63**, 1–5.

[3] Yarden Y and Sliwkowski MX (2001). Untangling the ErbB signalling network. *Nat Rev Mol Cell Biol* **2**, 127–137.

[4] Baselga J (2006). Targeting tyrosine kinases in cancer: the second wave. *Science* **312**, 1175–1178.

[5] Speake G, Holloway B, and Costello G (2005). Recent developments related to the EGFR as a target for cancer chemotherapy. *Curr Opin Pharmacol* **5**, 343–349.

[6] Aerts HJ, Dubois L, Hackeng TM, Straathof R, Chiu RK, Lieuwes NG, Jutten B, Weppler SA, Lammering G, Wouters BG, et al. (2007). Development and

evaluation of a cetuximab-based imaging probe to target EGFR and EGFRvIII. *Radiother Oncol* **83**, 326–332.

[7] Barrett T, Koyama Y, Hama Y, Ravizzini G, Shin IS, Jang BS, Paik CH, Urano Y, Choyke PL, and Kobayashi H (2007). *In vivo* diagnosis of epidermal growth factor receptor expression using molecular imaging with a cocktail of optically labeled monoclonal antibodies. *Clin Cancer Res* **13**, 6639–6648.

[8] Cai W, Chen K, He L, Cao Q, Koong A, and Chen X (2007). Quantitative PET of EGFR expression in xenograft-bearing mice using ^{64}Cu-labeled cetuximab, a chimeric anti-EGFR monoclonal antibody. *Eur J Nucl Med Mol Imaging* **34**, 850–858.

[9] Manning HC, Merchant NB, Foutch AC, Virostko JM, Wyatt SK, Shah C, McKinley ET, Xie J, Mutic NJ, Washington MK, et al. (2008). Molecular imaging of therapeutic response to epidermal growth factor receptor blockade in colorectal cancer. *Clin Cancer Res* **14**, 7413–7422.

[10] Schechter NR, Wendt RE III, Yang DJ, Azhdarinia A, Erwin WD, Stachowiak AM, Broemeling LD, Kim EE, Cox JD, Podoloff DA, et al. (2004). Radiation dosimetry of ^{99m}Tc-labeled C225 in patients with squamous cell carcinoma of the head and neck. *J Nucl Med* **45**, 1683–1687.

[11] Schechter NR, Yang DJ, Azhdarinia A, Kohanim S, Wendt R III, Oh CS, Hu M, Yu DF, Bryant J, Ang KK, et al. (2003). Assessment of epidermal growth factor receptor with ^{99m}Tc-ethylenedicysteine-C225 monoclonal antibody. *Anticancer Drugs* **14**, 49–56.

[12] Diagaradjane P, Orenstein-Cardona JM, Colon-Casasnovas NE, Deorukhkar A, Shentu S, Kuno N, Schwartz DL, Gelovani JG, and Krishnan S (2008). Imaging epidermal growth factor receptor expression *in vivo*: pharmacokinetic and biodistribution characterization of a bioconjugated quantum dot nanoprobe. *Clin Cancer Res* **14**, 731–741.

[13] Ke S, Wen X, Gurfinkel M, Charnsangavej C, Wallace S, Sevick-Muraca EM, and Li C (2003). Near-infrared optical imaging of epidermal growth factor receptor in breast cancer xenografts. *Cancer Res* **63**, 7870–7875.

[14] Kovar JL, Johnson MA, Volcheck WM, Chen J, and Simpson MA (2006). Hyaluronidase expression induces prostate tumor metastasis in an orthotopic mouse model. *Am J Pathol* **169**, 1415–1426.

[15] Velikyan I, Sundberg AL, Lindhe O, Hoglund AU, Eriksson O, Werner E, Carlsson J, Bergstrom M, Langstrom B, and Tolmachev V (2005). Preparation and evaluation of (68)Ga-DOTA-hEGF for visualization of EGFR expression in malignant tumors. *J Nucl Med* **46**, 1881–1888.

[16] Adams KE, Ke S, Kwon S, Liang F, Fan Z, Lu Y, Hirschi K, Mawad ME, Barry MA, and Sevick-Muraca EM (2007). Comparison of visible and near-infrared wavelength-excitable fluorescent dyes for molecular imaging of cancer. *J Biomed Opt* **12**, 024017.

[17] Cheng Z, De Jesus OP, Namavari M, De A, Levi J, Webster JM, Zhang R, Lee B, Syud FA, and Gambhir SS (2008). Small-animal PET imaging of human epidermal growth factor receptor type 2 expression with site-specific ^{18}F-labeled protein scaffold molecules. *J Nucl Med* **49**, 804–813.

[18] Lee SB, Hassan M, Fisher R, Chertov O, Chernomordik V, Kramer-Marek G, Gandjbakhche A, and Capala J (2008). Affibody molecules for *in vivo* characterization of HER2-positive tumors by near-infrared imaging. *Clin Cancer Res* **14**, 3840–3849.

[19] Orlova A, Magnusson M, Eriksson TL, Nilsson M, Larsson B, Hoiden-Guthenberg I, Widstrom C, Carlsson J, Tolmachev V, Stahl S, et al. (2006). Tumor imaging using a picomolar affinity HER2 binding Affibody molecule. *Cancer Res* **66**, 4339–4348.

[20] Tolmachev V, Nilsson FY, Widstrom C, Andersson K, Rosik D, Gedda L, Wennborg A, and Orlova A (2006). ^{111}In-benzyl-DTPA-ZHER2:342, an Affibody-based conjugate for *in vivo* imaging of HER2 expression in malignant tumors. *J Nucl Med* **47**, 846–853.

[21] Friedman M, Nordberg E, Hoiden-Guthenberg I, Brismar H, Adams GP, Nilsson FY, Carlsson J, and Stahl S (2007). Phage display selection of Affibody molecules with specific binding to the extracellular domain of the epidermal growth factor receptor. *Protein Eng Des Sel* **20**, 189–199.

[22] Nordberg E, Friedman M, Gostring L, Adams GP, Brismar H, Nilsson FY, Stahl S, Glimelius B, and Carlsson J (2007). Cellular studies of binding, internalization and retention of a radiolabeled EGFR-binding Affibody molecule. *Nucl Med Biol* **34**, 609–618.

[23] Nordberg E, Orlova A, Friedman M, Tolmachev V, Stahl S, Nilsson FY, Glimelius B, and Carlsson J (2008). *In vivo* and *in vitro* uptake of ^{111}In, delivered with the Affibody molecule (ZEGFR:955)2, in EGFR expressing tumour cells. *Oncol Rep* **19**, 853–857.

[24] Tolmachev V, Friedman M, Sandstrom M, Eriksson TL, Rosik D, Hodik M, Stahl S, Frejd FY, and Orlova A (2009). Affibody molecules for epidermal growth factor receptor targeting *in vivo*: aspects of dimerization and labeling chemistry. *J Nucl Med* **50**, 274–283.

[25] Kovar JL, Simpson MA, Schutz-Geschwender A, and Olive DM (2007). A systematic approach to the development of fluorescent contrast agents for optical imaging of mouse cancer models. *Anal Biochem* **367**, 1–12.

[26] Massoud TF and Gambhir SS (2003). Molecular imaging in living subjects: seeing fundamental biological processes in a new light. *Genes Dev* **17**, 545–580.

[27] Weissleder R (2001). A clearer vision for *in vivo* imaging. *Nat Biotechnol* **19**, 316–317.

[28] Kovar JL, Volcheck W, Sevick-Muraca E, Simpson MA, and Olive DM (2009). Characterization and performance of a near-infrared 2-deoxyglucose optical imaging agent for mouse cancer models. *Anal Biochem* **384**, 254–262.

[29] Cheng Z, Levi J, Xiong Z, Gheysens O, Keren S, Chen X, and Gambhir SS (2006). Near-infrared fluorescent deoxyglucose analogue for tumor optical imaging in cell culture and living mice. *Bioconjug Chem* **17**, 662–669.

[30] Ntziachristos V, Schellenberger EA, Ripoll J, Yessayan D, Graves E, Bogdanov A Jr, Josephson L, and Weissleder R (2004). Visualization of antitumor treatment by means of fluorescence molecular tomography with an annexin V–Cy5.5 conjugate. *Proc Natl Acad Sci USA* **101**, 12294–12299.

[31] Chen X, Conti PS, and Moats RA (2004). *In vivo* near-infrared fluorescence imaging of integrin $\alpha_v\beta_3$ in brain tumor xenografts. *Cancer Res* **64**, 8009–8014.

[32] Nitin N, Rosbach KJ, El-Naggar A, Williams M, Gillenwater A, and Richards-Kortum RR (2009). Optical molecular imaging of epidermal growth factor receptor expression to improve detection of oral neoplasia. *Neoplasia* **11**, 542–551.

[33] Sampath L, Kwon S, Ke S, Wang W, Schiff R, Mawad ME, and Sevick-Muraca EM (2007). Dual-labeled trastuzumab-based imaging agent for the detection of human epidermal growth factor receptor 2 overexpression in breast cancer. *J Nucl Med* **48**, 1501–1510.

[34] Urano Y, Asanuma D, Hama Y, Koyama Y, Barrett T, Kamiya M, Nagano T, Watanabe T, Hasegawa A, Choyke PL, et al. (2009). Selective molecular imaging of viable cancer cells with pH-activatable fluorescence probes. *Nat Med* **15**, 104–109.

[35] Gong H, Singh SV, Singh SP, Mu Y, Lee JH, Saini SP, Toma D, Ren S, Kagan VE, Day BW, et al. (2006). Orphan nuclear receptor pregnane X receptor sensitizes oxidative stress responses in transgenic mice and cancerous cells. *Mol Endocrinol* **20**, 279–290.

[36] Gong H, Zhang B, Little G, Kovar J, Chen H, Xie W, Schutz-Geschwender A, and Olive DM (2009). β-Galactosidase activity assay using far-red–shifted fluorescent substrate DDAOG. *Anal Biochem* **386**, 59–64.

[37] Gong H, Jarzynka MJ, Cole TJ, Lee JH, Wada T, Zhang B, Gao J, Song WC, DeFranco DB, Cheng SY, et al. (2008). Glucocorticoids antagonize estrogens by glucocorticoid receptor–mediated activation of estrogen sulfotransferase. *Cancer Res* **68**, 7386–7393.

[38] Matar P, Rojo F, Cassia R, Moreno-Bueno G, Di Cosimo S, Tabernero J, Guzman M, Rodriguez S, Arribas J, Palacios J, et al. (2004). Combined epidermal growth factor receptor targeting with the tyrosine kinase inhibitor gefitinib (ZD1839) and the monoclonal antibody cetuximab (IMC-C225): superiority over single-agent receptor targeting. *Clin Cancer Res* **10**, 6487–6501.

[39] Friedman M, Orlova A, Johansson E, Eriksson TL, Hoiden-Guthenberg I, Tolmachev V, Nilsson FY, and Stahl S (2008). Directed evolution to low nanomolar affinity of a tumor-targeting epidermal growth factor receptor-binding Affibody molecule. *J Mol Biol* **376**, 1388–1402.

[40] Moasser MM, Basso A, Averbuch SD, and Rosen N (2001). The tyrosine kinase inhibitor ZD1839 ("Iressa") inhibits HER2-driven signaling and suppresses the growth of HER2-overexpressing tumor cells. *Cancer Res* **61**, 7184–7188.

[41] Weissleder R and Pittet MJ (2008). Imaging in the era of molecular oncology. *Nature* **452**, 580–589.

[42] Willmann JK, van Bruggen N, Dinkelborg LM, and Gambhir SS (2008). Molecular imaging in drug development. *Nat Rev Drug Discov* **7**, 591–607.

[43] Dennis MS, Jin H, Dugger D, Yang R, McFarland L, Ogasawara A, Williams S, Cole MJ, Ross S, and Schwall R (2007). Imaging tumors with an albumin-binding Fab, a novel tumor-targeting agent. *Cancer Res* **67**, 254–261.

[44] Stoscheck CM and King LE Jr (1986). Role of epidermal growth factor in carcinogenesis. *Cancer Res* **46**, 1030–1037.

[45] Komuves LG, Feren A, Jones AL, and Fodor E (2000). Expression of epidermal growth factor and its receptor in cirrhotic liver disease. *J Histochem Cytochem* **48**, 821–830.

[46] Koyama Y, Barrett T, Hama Y, Ravizzini G, Choyke PL, and Kobayashi H (2007). *In vivo* molecular imaging to diagnose and subtype tumors through receptor-targeted optically labeled monoclonal antibodies. *Neoplasia* **9**, 1021–1029.

[47] Kobayashi H, Koyama Y, Barrett T, Hama Y, Regino CA, Shin IS, Jang BS, Le N, Paik CH, Choyke PL, et al. (2007). Multimodal nanoprobes for radionuclide and five-color near-infrared optical lymphatic imaging. *ACS Nano* **1**, 258–264.

[48] Tolmachev V, Rosik D, Wallberg H, Sjoberg A, Sandstrom M, Hansson M, Wennborg A, and Orlova A (in press). Imaging of EGFR expression in murine xenografts using site-specifically labelled anti-EGFR (111)In-DOTA-Z (EGFR:2377) Affibody molecule: aspect of the injected tracer amount. *Eur J Nucl Med Mol Imaging*.

[49] Tolmachev V, Orlova A, Pehrson R, Galli J, Baastrup B, Andersson K, Sandstrom M, Rosik D, Carlsson J, Lundqvist H, et al. (2007). Radionuclide therapy of HER2-positive microxenografts using a ^{177}Lu-labeled HER2-specific Affibody molecule. *Cancer Res* **67**, 2773–2782.

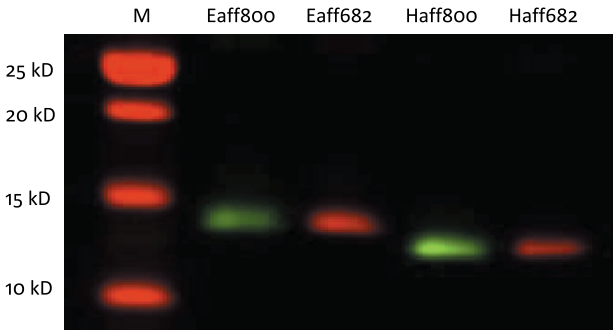

Figure W1. Gel image of Affibody molecules labeled with IR-Dye800CW or DY-682. Labeled Affibody molecules were purified by passing reaction mixture through a Zeba Spin Desalting Column. Purified samples (0.2 pmol each) were separated on a Bis-Tris gel.

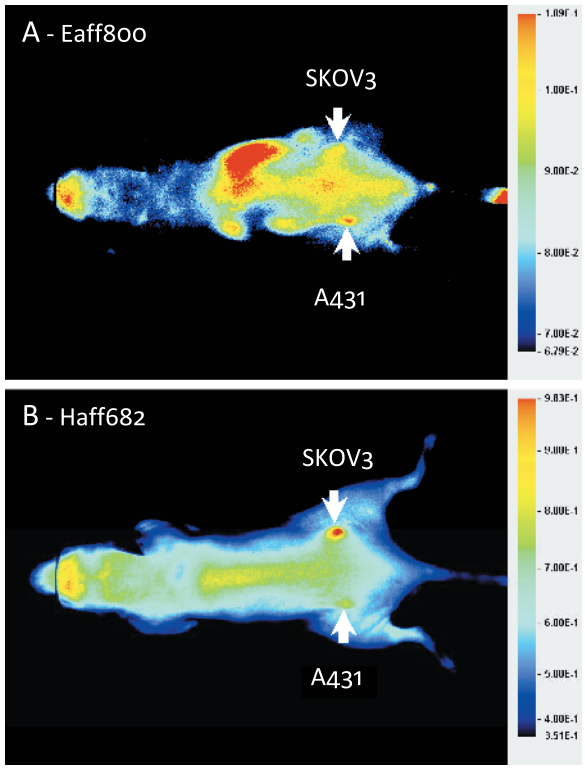

Figure W2. Pseudocolored images of mouse with Eaff800 signal (A) or Haff682 signal (B). Note that S2A and S2B were pseudocolored images of Figure 6, *A-a* and *A-b*, respectively. See Figure 6 for details of experiment.

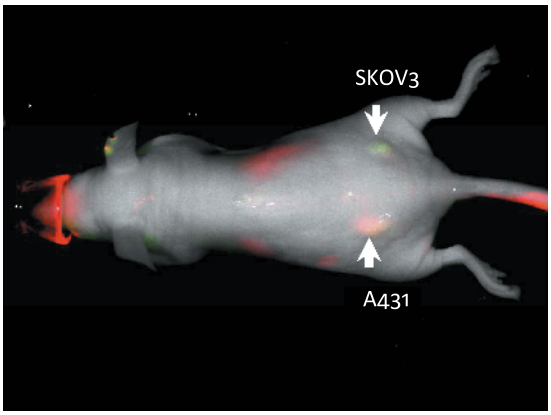

Figure W3. Two-color *in vivo* optical imaging with Eaff682 and Haff800. Nude mice bearing A431 and SKOV3 tumors on the left and right sides, respectively, were injected with 100 μl of PBS containing 0.5 nmol of Eaff682 and 0.5 nmol of Haff800. Whole body images (dorsal view) were acquired 1 day after agent injection. Green and red represent IRDye800CW and DY-682 fluorescence signals, respectively. The tumors are indicated with arrows.

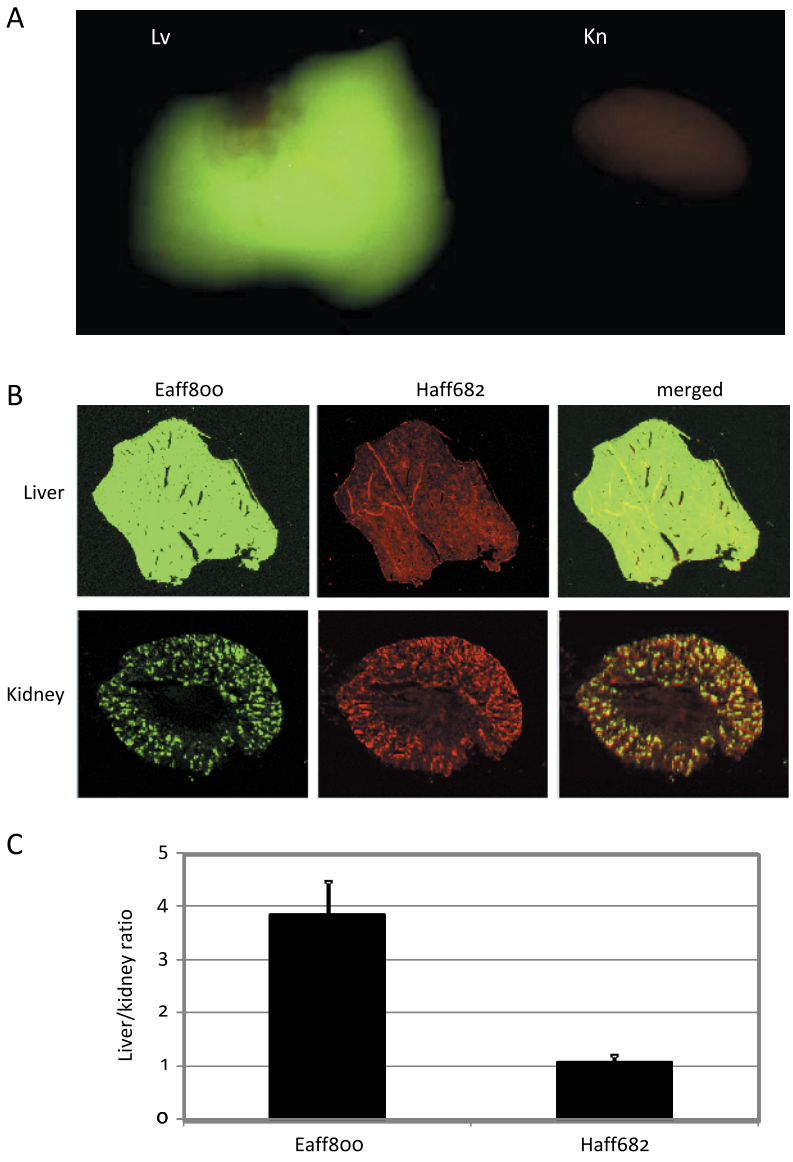

Figure W4. Accumulation of Eaff800 and Haff682 in mouse liver and kidney. (A) Images of the liver and kidney. Mice were killed 1 day after imaging agent injection. The organs were collected and rinsed in PBS before imaging. Green and red represent IRDye800CW and DY-682 fluorescence signals, respectively. *Kn* indicates kidney; *Lv*, liver. (B) Sections of mouse liver and kidney. The organs were snap-frozen in OCT compound and sectioned at 8-μm thickness. (C) Liver-to-kidney ratio of Eaff800 and Haff682 signal intensities. Average signal intensities were calculated using ROIs with the same sizes from different tissue sections. Liver-to-kidney ratio was calculated by dividing liver signal intensity by kidney signal intensity.

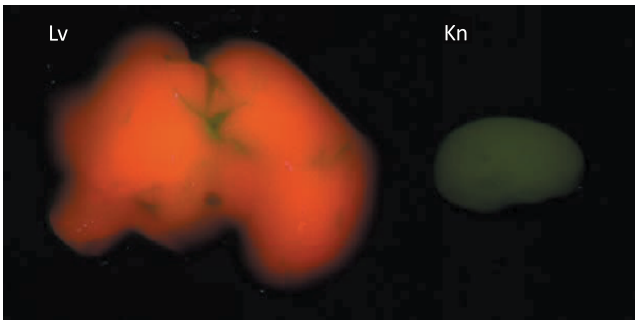

Figure W5. Accumulation of Eaff682 and Haff800 in mouse liver and kidney. Mice were killed 1 day after imaging agent injection. The liver and kidney were collected and rinsed in PBS before imaging. Green and red represent IRDye800CW and DY-682 fluorescence signals, respectively. Note the predominant Eaff682 signal in the liver. *Kn* indicates kidney; *Lv*, liver.